A Rigorous Measure of the Complexity of Neural Representations based on Partial Information Decomposition

Anonymous authors
Paper under double-blind review

Abstract

In neural networks, task-relevant information is represented jointly by groups of neurons. However, the specific way in which the information about the classification label is distributed among the individual neurons is not well understood: While parts of it may only be obtainable from specific single neurons, other parts are carried redundantly or synergistically by multiple neurons. We show how Partial Information Decomposition (PID), a recent extension of information theory, can disentangle these different contributions. From this, we introduce the measure of "Representational Complexity", which quantifies the difficulty of accessing information spread across multiple neurons. We show how this complexity is directly computable for smaller layers. For larger layers, we propose subsampling and coarse-graining procedures and prove corresponding bounds on the latter. Empirically, for quantized deep neural networks solving the MNIST and CIFAR10 tasks, we observe that representational complexity decreases both through successive hidden layers and over training. Overall, we propose representational complexity as a principled and interpretable summary statistic for analyzing the structure and evolution of neural representations and complex systems in general.

1 Introduction

Despite their tremendous success, the inner workings of artificial neural networks remain mostly elusive to this date (LeCun et al., 2015; Alom et al., 2019; Samek et al., 2017). It is known that, since all of the information a network can use to solve a task must already be contained in the model's inputs, the purpose of hidden internal components remains to distill the pertinent features and make them available to later computational steps. However, the *way* in which the features are represented among multiple neurons and how this representation changes throughout the training phase is not well understood (Li et al., 2015; Bengio et al., 2013). This lack of understanding continues to pose a major obstacle to the adoption of machine learning techniques in critical settings, such as medical image analysis or self-driving cars, but also hinders principled development of better machine learning algorithms (Samek et al., 2017; Amodei et al., 2016; Eykholt et al., 2018).

In a classification problem, the difficulty of extracting information about the target label from internal representations in hidden layers is a key factor for network performance and interpretability alike. As a first step towards these objectives, one needs to rigorously define and quantify this notion of *difficulty*, which originates from complex higher-order statistical interrelations between neurons. These relations – if present – make it necessary to consider large groups of neurons at a time to be able to discriminate between certain represented target values. The number of neurons minimally needed to obtain a piece of target-discriminatory information is conceptually related to the classical question of how many neurons are active in the representation of an input sample, and may thus be viewed as an information-theoretic equivalent of a sparsity measure. We propose to quantify this 'information sparsity' in a principled way by answering an intuitive question: On average, how many neurons do I need to observe simultaneously in order to gain access to a piece of information? Note that while we limit ourselves to classification problems in this paper, these questions pertain to a vast class of problems not limited to machine learning systems wherever information about some target variable is distributed amongst a set of equivalent information bearing units.

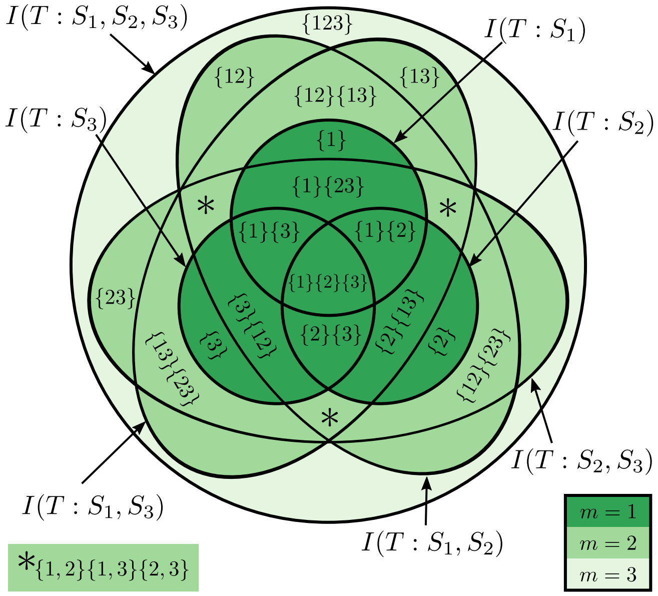

Figure 1: **Mereological diagram illustrating how the PID atoms $\Pi(T:\boldsymbol{S}_\alpha)$ constitute all classical mutual information quantities involving three source variables, as introduced by Williams and Beer (2010).** Classical mutual information terms are represented by black ovals with general redundancies given by their overlaps. The PID atoms correspond to the contiguous areas of the overlaps and are labelled by their corresponding antichains α. The green shading indicates the degree of synergy m of the respective atoms.

From the perspective of Information Theory (Shannon, 1948), neural networks are just information channels that forward the task-relevant part of the input to the output layer while shedding task-irrelevant parts (Tishby and Zaslavsky, 2015). This said, the idea of using information theory to quantify the information in the activations of Deep Neural Network (DNN) hidden layers has been met with fierce debate after methodological flaws surfaced (Saxe et al., 2019; Goldfeld et al., 2019) in the influential early works by Tishby et al. (Tishby and Zaslavsky, 2015; Shwartz-Ziv and Tishby, 2017). We address these issues in this work and show how information theory can be applied to quantized networks in a theoretically sound way.

Yet, even with such methodological problems out of the way, the question posed above on how features are represented cannot be answered using classic information theory alone. This is due to the inability of classic information theory to disentangle redundant and synergistic contributions between multiple neurons (Williams and Beer, 2010), leading to inevitable double- or under-counting of information contributions. Non-overlapping information contributions can be obtained by decomposing the mutual information $I(T:\boldsymbol{S})$ between a target random variable T and several source variables $\boldsymbol{S}=(S_1,\ldots,S_n)$ into its information *atoms* $\Pi(T:\boldsymbol{S}_\alpha)$ such that

$$I(T:\boldsymbol{S})=\sum_\alpha \Pi(T:\boldsymbol{S}_\alpha), \tag{1}$$

which has been made possible by the introduction of a recent extension to information theory known as Partial Information Decomposition (PID) (Williams and Beer, 2010). These atoms are the smallest set of quantities from which the mutual information between T and all possible subsets of $\boldsymbol{S}$ can be combined (Figure 1) (Gutknecht et al., 2021). Note that here, each information atom is referred to by its corresponding 'antichain' α, which will be explained in Section 3.1.

From the PID atoms, we can answer the question of how many neurons are needed to access an average piece of information in a principled way by introducing the summary statistic we term "Representational Complexity". A representational complexity of $C=1$ means that all information can be obtained from single neurons, while a representational complexity C that is equal to the number of neurons in a layer means that no information can be obtained about the target unless one has access to all neurons. By tracking the representational complexity C of the hidden layers over training we shed light upon a key aspect of how the internal representations of the target variable evolve during the training phase. This understanding may subsequently be employed to improve network designs by providing a tool to compare the dynamics in different network architectures.

The main contributions of this work are **(i)** describing a principled approach for applying PID to analyze the representations in DNNs and related systems, **(ii)** the introduction of representational complexity as a measure of information sparsity, **(iii)** discussing subsampling and coarse-graining procedures for the estimation of representational complexity and proofs of bounds on the latter and **(iv)** empirical results in quantized DNNs showing a decrease in representational complexity over training and through successive hidden layers.

2 Related works

Tishby and Zaslavsky (2015) were among the first to attempt to analyze deep neural networks from an information-theoretic perspective. Information theory, which was developed for the analysis of noisy information channels (Shannon, 1948), allows to quantify information in an observer-independent way and helps to form a clear criterion of relevancy of information in hidden representations by distinguishing between the mutual information of layer activations with the ground truth classification labels and with the input variables. Viewing the networks as a sequence of such channels, Shwartz-Ziv and Tishby (2017) computed mutual information from *binned* activations of the individual hidden layers, and plotted the resulting trajectory in what they termed the *information plane.* This information plane is a two-dimensional space with the mutual information between hidden layer activations and input, and between hidden layer activations and ground-truth label as its two dimensions.

However, their claim to estimate actual mutual information quantities of the network variables with their binning approach was later shown to be unfounded (Saxe et al., 2019; Goldfeld et al., 2019). In fact, the true mutual information between the network's inputs or label and a hidden layer is either infinite, in the case of continuous features, or constant and equal to the finite entropy of the discrete inputs or labels (Saxe et al., 2019; Goldfeld et al., 2019; Geiger, 2021). This is due to the fact that the network itself defines a deterministic and almost always injective mapping from inputs to hidden layer activation values. For this reason, the results shown by Shwartz-Ziv and Tishby (2017) do not constitute estimates of actual information-theoretic quantities and may at best be reinterpreted as measures for geometric clustering (Goldfeld et al., 2019; Geiger, 2021).

Building on this realization, Goldfeld et al. (2019) showed that a meaningful information-theoretic analysis can be performed by disrupting the injectivity and limiting the channel capacity of the network forward function. While they achieve this by explicitly adding Gaussian noise to each activation value, we achieve the same goal by training and analyzing quantized very-low precision activation values in this work. This approach is in line with recent trends towards low (Gupta et al., 2015) and very-low precision (Hubara et al., 2017) computing for reasons of efficiency and scalability. The crucial difference to Shwartz-Ziv and Tishby (2017)'s binning approach lies in the fact that the quantization we employ is intrinsic to the network itself, making mutual information quantities well-defined and meaningful as well as ensuring the data processing inequality holds for the Markov chain of successive hidden layers.

The picture of artificial neural networks as mere information channels needs to be refined following the insight that network layers need not only to pass on all relevant information, but also to transform it in such a way that it becomes accessible for subsequent processing. To understand this representation of information within each layer, one needs to go beyond analyzing hidden layers as a whole and look at the structure of information representation across the neurons within those layers instead, which can be done in a principled way by employing partial information decomposition.

Previous works on PID in artificial neural networks have used PID to motivate and interpret classical mutual information quantities (Wibral et al., 2017) and used it to analyze filters in convolutional neural networks (Yu et al., 2020). Furthermore, Tax et al. (2017) used PID to analyze pairs of neurons in generative neural networks and find that the networks move towards more unique representations of the target in later stages of training. We expand upon this approach by being the first to analyze all neurons of a layer as individual PID sources, which allows also to uncover higher-order interactions between them.

Closely connected to our approach, Reing et al. (2021) derived scalable measures for quantifying higher-order interactions between neurons using information theory. By focusing more on scalability, however, the authors trade in some of the interpretability and expressivity of an approach based on PID. Furthermore, Reing et al. (2021) cover mostly the analysis of representations without reference to a target variable, while we focus on analyzing only task-relevant information contributions.

In the context of representation learning, information-theoretic approaches focus mostly on quantifying the degree of entanglement of latent dimensions in Variational Autoencoders, often with respect to the information about some underlying generative factor. This is done by measuring the total correlation (Kim and Mnih, 2018) as a summary statistic or the difference between two classical mutual information quantities (Chen et al., 2018; Tokui and Sato, 2021). These works are related to ours, but analyze only a specific layer, do not use the label information as target and stay within the realm of classical information theory.

Other works on representations in deep neural networks have attempted to define notions of *usable* information based on the idea of restricting the ability of an observer to perfectly decode the presented information (Xu et al., 2019; Kleinman et al., 2020). A related approach is the probing of representations using simple linear readouts, for example Alain and Bengio (2017), who find empirical evidence hinting at less complex representations in deeper layers. Additionally, several other summary statistics of representations have been suggested based on dimensionality analysis (Ansuini et al., 2019) or canonical correlation analysis (Morcos et al., 2018; Kornblith et al., 2019).

Several other complexity measures were compared by Jiang et al. (2019), who analyzed them in terms of their ability to predict the networks' capacities for out-of-sample generalization. This idea is founded on the intuitive notion that less complex representations should be more robust to minor changes in the inputs. As our paper is focused on interpretability and theoretical soundness of the novel measure of representational complexity, potential ties to generalization ability have not been studied as of yet.

3 Deriving an interpretable measure for the complexity of a representation from partial information decomposition

3.1 Partial information decomposition

The mutual information $I(T : \boldsymbol{S}) = I(T : S_1, \ldots, S_n)$ that several source random variables $\boldsymbol{S} = \{S_1, \ldots, S_n\}$ carry about a target T can be distributed amongst these sources in very different ways. While some pieces of information are *unique* to certain sources, others are encoded *redundantly* by different sources, while yet others are only accessible *synergistically* from several sources considered jointly. With three or more sources, even more complex contributions, in general describing redundancies between synergies, emerge. For example, some information about T might be accessible either from source S_3 alone, or – redundantly to this – from a synergistic combination of sources S_1 and S_2, but from nowhere else; this information would constitute one of the information atoms Π.

As mentioned before, these information atoms can be combined to form all classical mutual information quantities $I(T : \boldsymbol{S_a})$ between T and subsets of sources $\boldsymbol{S_a} = \{S_i | i \in \boldsymbol{a}\}$ with indices $\boldsymbol{a} \subseteq \{1, \ldots, n\}$. Conversely, the information atoms can be uniquely identified by which classical mutual information quantities they contribute to. Mathematically, this notion is captured by their corresponding *parthood distribution* $\Phi : \mathcal{P}(\{1, \ldots, n\}) \to \{0, 1\}$ – a binary function defined on the powerset $\mathcal{P}$ of source indices that is equal to "1" for exactly those sets $\boldsymbol{a}$ of source indices for which the atom $\Pi(T : \boldsymbol{S}_\Phi)$ is part of the mutual information $I(T : \boldsymbol{S_a})$ (Gutknecht et al., 2021). Thus, the mutual information of any set of sources $\boldsymbol{S_a}$ and T can be written as

$$I(T : \boldsymbol{S_a}) = \sum_{\{\Phi | \Phi(\boldsymbol{a})=1\}} \Pi(T : \boldsymbol{S}_\Phi). \tag{2}$$

Instead of labelling the atoms by their parthood distribution Φ, the atoms can equivalently be referenced as $\Pi(T : \boldsymbol{S}_\alpha)$ using certain sets of sets of source indices $\alpha \in \mathcal{P}(\mathcal{P}(\{1, \ldots, n\}))$, which can be mapped one-to-one to parthood distributions (Gutknecht et al., 2021) and are referred to as *antichains* (Williams and Beer, 2010) (see Appendix A.1). The antichains make apparent the connection between atoms and their meaning as redundancies between synergies: For example, the atom from before capturing the information that can be obtained either from S_3 alone or synergistically from S_1 and S_2 together is referred to by the antichain $\{\{1, 2\}, \{3\}\}$.

The number of atoms scales super-exponentially with the number of sources n, increasing from 7579 for $n = 5$ sources to over 7.8 million for $n = 6$ (Williams and Beer, 2010; Wiedemann, 1991). Note, however, that this increase in the number of atoms should not be mistaken for a shortcoming of PID but rather as an acknowledgement of the vast number of configurations information can be encoded in amongst multiple variables.

On the other hand, there are only $2^n - 1$ classical information quantities that provide constraints through Equation (2). One way to resolve this underdeterminedness is through the introduction of a measure for redundancy $I_\cap(T : \boldsymbol{S}_\alpha) = I_\cap(T : \{\boldsymbol{S}_{\boldsymbol{a}_1}, \ldots, \boldsymbol{S}_{\boldsymbol{a}_k}\})$ between collections of sources indexed by $\boldsymbol{a}_i \subseteq \{1, \ldots, n\}$. Noting that mutual information can be interpreted as a "self-redundancy" such that $I(T : \boldsymbol{S}_{\boldsymbol{a}}) = I_\cap(T : \{\boldsymbol{S}_{\boldsymbol{a}}\})$, these redundancies can be constructed from the information atoms in an analogous and consistent way to Equation (1) as

$$I_\cap(T : \boldsymbol{S}_\alpha) = \sum_{\beta \preceq \alpha} \Pi(T : \boldsymbol{S}_\beta), \tag{3}$$

where $\preceq$ refers to the partial order of antichains on the redundancy lattice (see Appendix A.2) (Crampton and Loizou, 2000; 2001; Williams and Beer, 2010). Since now the number of defining equations is equal to the number of atoms, these can be computed by inverting Equation (3), which is known as a *Moebius-Inversion* (Rota, 1964; Williams and Beer, 2010).

Over recent years, a number of different redundancy measures have been suggested which fulfill a multitude of different additional desiderata (Lizier et al., 2018), e.g., from decision theory (Bertschinger et al., 2014), game theory (Ince, 2017) or Kelly gambling (Finn and Lizier, 2018). In this paper, we utilize the $I_\cap^{\text{sx}}$ measure introduced by Makkeh et al. (2021), where 'sx' stands for shared exclusions of probability mass. In essence, the measure defines redundancy by the regions of probability space which are jointly excluded by observing the realizations of multiple collections of random variables. As this redundancy measure draws only on notions from probability theory it is the most canonical choice for our purpose of analyzing neural networks. The concept of representational complexity that we introduce here, however, can readily be generalized to any other redundancy-based multivariate PID.

3.2 Representational complexity

In order to gain insight into the representation of task-relevant information in multiple equivalent source variables, we introduce in the following a principled way to evaluate the question: How much of a system needs to be observed simultaneously to access a particular piece of information? We propose that this difficulty of retrieving information may be quantified by considering the minimum number of sources that are needed jointly in order to reveal a piece of information. As a first step towards this goal, one needs to dissect the total mutual information into pieces which individually have a clear notion of how many neurons are needed to retrieve the information.

Note, however, that such a dissection cannot be achieved with classical information theory due to its inability to disentangle synergistic and redundant contributions: As an example, take two source variables S_1 and S_2 which carry information about a target T. Since the mutual information term $I(T : S_i)$ captures all information that the single source S_i carries about T, one might think that the total information that can be obtained from single sources is given by the sum $I(T : S_1) + I(T : S_2)$. However, apart from their individual unique contributions, S_1 and S_2 might carry some identical pieces of information about T, and this redundancy is double-counted in the above sum. The joint mutual information $I(T : S_1, S_2)$, on the other hand, consists of four atoms: The two unique atoms of the respective sources, their redundancy and their synergy. Thus, if we subtract the sum of the individual mutual information terms from the joint term we obtain

$$I(T : S_1, S_2) - I(T : S_1) - I(T : S_2) = \text{synergy} - \text{redundancy},$$

with no way to quantify synergy or redundancy individually. Since the redundancy can be obtained from any single variable while the synergy necessarily requires access to both variables jointly, it is impossible to dissect the joint mutual information into pieces with a well-defined minimal number of neurons needed to retrieve the information from classical information theory alone.

The PID atoms, on the other hand, do have a well-defined minimal number of neurons necessary to retrieve the information, which is captured by the "Degree of Synergy" m given by

$$m(\alpha) := \min_{\boldsymbol{a} \in \alpha} |\boldsymbol{a}|, \tag{4}$$

which is illustrated for all trivariate PID atoms in Figure 1. For instance, the PID atom with the antichain $\{1\}\{4\}\{2,3\}$ has a degree of synergy of $m = 1$ since the information can be obtained by observing the single sources S_1 or S_4, while the atom with the antichain $\{1,2\}\{3,4,5\}$ has a degree of synergy of $m = 2$ since the smallest set of sources the information can be retrieved from is the pair consisting of S_1 and S_2.

Finally, the average degree of synergy, weighted by the relative information contributions of the respective atoms, defines the "Representational Complexity" C as

$$C := \frac{1}{I(T : \boldsymbol{S})} \sum_{\alpha} \Pi(T : \boldsymbol{S}_\alpha)\, m(\alpha). \tag{5}$$

A representational complexity of $C = 1$ means that all information can be obtained from single sources, while C is equal to the number of sources if the information is spread purely synergistically between all of them.

The concept of representational complexity is linked to the idea of sparse coding in neuroscience (Olshausen and Field, 2004), in that both approaches aim to capture the relevancy of higher-order relations between neurons. While sparsity measures quantify the spread of activity tied to individual realizations across the neuron population, e.g., by measuring the momentary average of non-zero neurons, representational complexity measures the spread of *information*, i.e., how distributed the ability to *distinguish between* realizations of the target variable (e.g. the label in classification tasks) is. Note further that representational complexity is computed on the mutual information with the network's target variable, thus relating to only task-relevant components of the activation patterns, while sparsity measures are generally not selective about the task-relevancy of the activations.

Example applications of representational complexity To become familiar with the intuitive interpretation of representational complexity, we demonstrate its use with simple information encodings in small toy examples. Consider a categorical random variable with a finite number of distinct classes, which are labelled by integers and occur with the same probability. How does representational complexity differ between different representations of this information in multiple binary neurons?

First, imagine four distinct values are represented sparsely across four neurons (Figure 2.A). As for all such *one-hot* encodings, the representational complexity of this encoding is equal to one (Appendix A.4). This is intuitively clear: For each realization, you only need access to the one neuron that is equal to 1 to fully determine the correct label.

Using the same number of neurons, we can also encode the same information in a more complex way. For instance, take pairs of neurons that redundantly represent digits of a binary representation of the label index (Figure 2.B). In this case, there is no longer a single neuron that contains the full information about the target, which is reflected by an increase of the representational complexity to $C = 1.21$.

Using all of the coding capacity of the four neurons from the example before by encoding 16 distinct states in a binary code (Figure 2.C), the representational complexity increases further: C reaches a value of 1.67

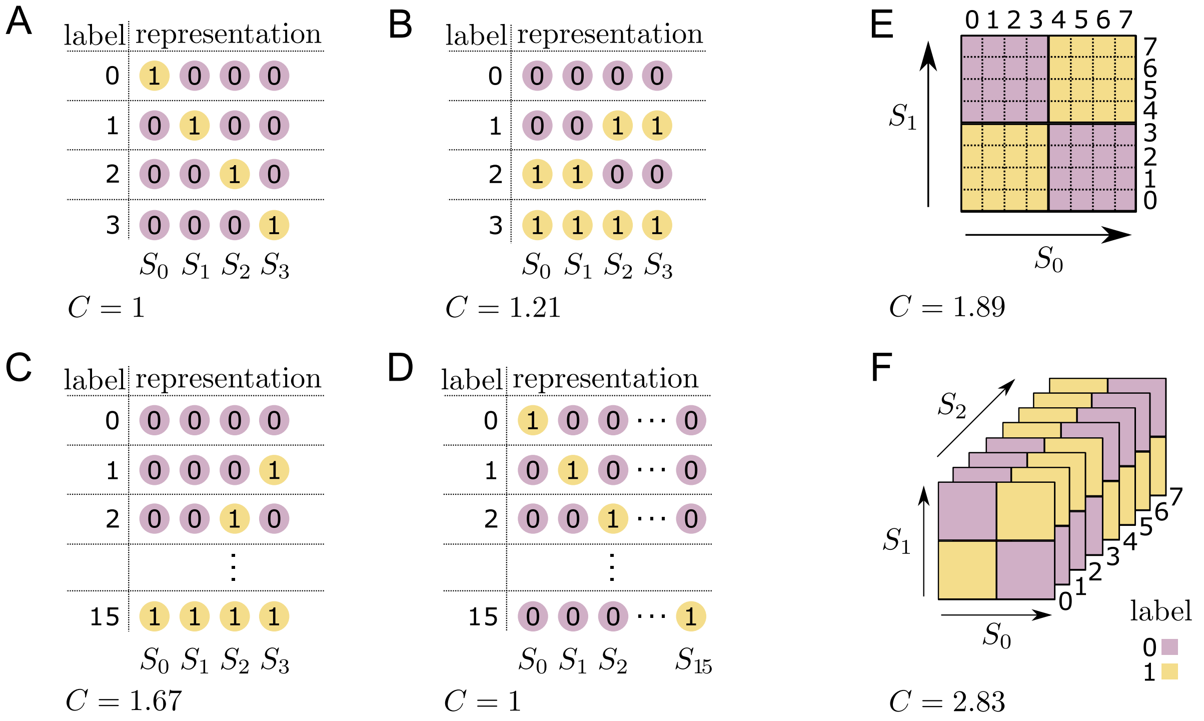

A

label	S_0	S_1	S_2	S_3
0	1	0	0	0
1	0	1	0	0
2	0	0	1	0
3	0	0	0	1

$C = 1$

B

label	S_0	S_1	S_2	S_3
0	0	0	0	0
1	0	0	1	1
2	1	1	0	0
3	1	1	1	1

$C = 1.21$

C

label	S_0	S_1	S_2	S_3
0	0	0	0	0
1	0	0	0	1
2	0	0	1	0
		⋮		
15	1	1	1	1

$C = 1.67$

D

label	S_0	S_1	S_2		S_{15}
0	1	0	0	···	0
1	0	1	0	···	0
2	0	0	1	···	0
		⋮			
15	0	0	0	···	1

$C = 1$

Figure 2: **Demonstration of representational complexity with simple examples.** Subfigures **A-D** show different label encoding schemes in binary neurons $S_1, \ldots, S_n$ (circles). Subfigure **E** shows an encoding of two labels (purple and yellow) in two eight-level neurons, while **F** shows the three-dimensional extension. The corresponding representational complexities C are denoted in the bottom left corner.

as more information has to be encoded synergistically between the four neurons. The reason why C is not equal to 4, despite the fact that the correct label can only be isolated with access to all four neurons, is that *parts* of the information, e.g., the parity of the label number, can be extracted from fewer than all sources. Conversely, if we now again expand the 16 realizations to 16 neurons in a one-hot encoding (Figure 2.D), we revert back to a representational complexity of just $C = 1$. From this, we gain the intuitive realization that the closer one gets to the channel capacity, the more one is forced to encode some of the information in more complex, higher-synergy terms.

However, even small amounts of information can be encoded in a highly synergistic manner. Consider the more realistic case of two discrete artificial neurons with eight activation levels each, with the target value being the exclusive disjunction (XOR) of the thresholded neurons' activations (Figure 2.E). Despite encoding just a single bit of information, the representational complexity assumes a value of $C = 1.89$. This value is close to the theoretical maximum value of $C = n = 2$, with the small difference being due to the nature of the $I_\cap^{\text{sx}}$ redundancy measure. Extending this task to the parity of three thresholded neurons (Figure 2.F), the representational complexity attains a value of $C = 2.83$, similarly close to its maximum of $C = n = 3$.

4 Application to deep neural networks

To exemplify the utility of our measure, we show how it can be applied to analyze the hidden layer representations of deep neural network classifiers solving the well-established MNIST (LeCun et al., 1998) handwritten digit recognition and CIFAR10 (Krizhevsky, 2009) image classification tasks. For the former, we employ a small fully-connected feed-forward network of which we analyze the last four layers before the output layer while for the latter we employ a more sophisticated convolutional network architecture and analyze the final small fully-connected layers.

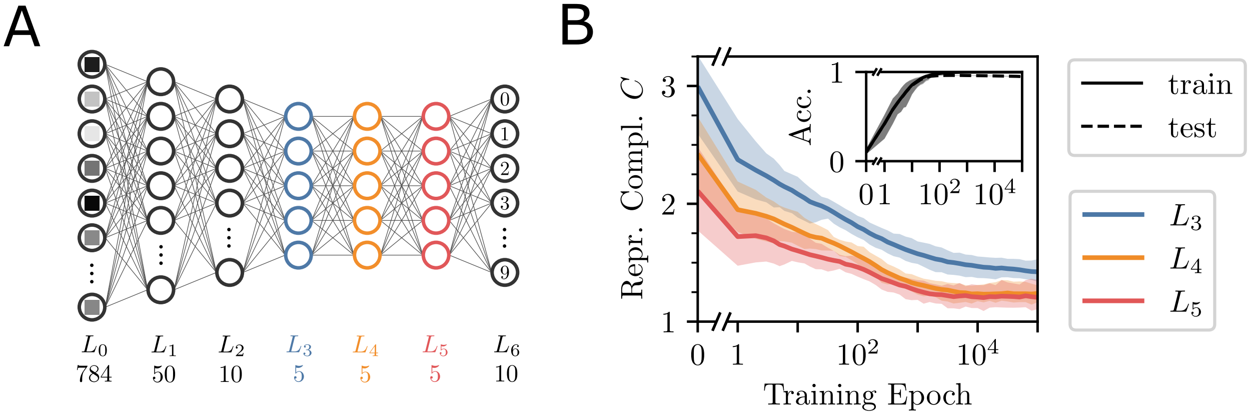

Figure 3: **Representational complexity of hidden layers with respect to the label decreases over training and throughout successive hidden layers. A** The MNIST classifier network consists of seven fully-connected layers with tanh activation functions for all but the last layer, which is equipped a softmax activation function. **B** The representational complexity of the three small hidden layers L_3, L_4 and L_5 are computed from their PID atoms on the train data set. The solid lines show the average of 20 randomly initialized runs, the shaded areas contain 95% of the data points. The inset shows train and test set accuracy.

The MNIST network consists of seven fully-connected layers, starting with a vector of the 784 grayscale pixel values of the image input, tapering down to only five neurons in layers L_3, L_4 and L_5 and culminating in a ten neuron *one-hot* output vector, in which each neuron represents one of the ten possible digits (Figure 3.A). The structure has been chosen such that the three successive five-neuron layers can be analyzed in full, as it is practically infeasible at present to compute the full PID for more than five sources because of the fast-growing number of PID atoms.

In order to limit the channel capacity to be able to observe non-trivial information dynamics (Goldfeld et al., 2019), all layers are discretized to eight or four quantization levels (3 or 2 bits) per neuron during both training and analysis (Appendix A.5). The networks are trained using stochastic gradient descent for 10^5 training epochs and reach, with eight quantization levels, an average accuracy of 99.9(1) % on the train and 95.1(4) % on the test set for 20 runs with unique random weight initializations. Details about quantization schemes and forward-stochastic backprop algorithm used in training can be found in Appendix A.5.

The larger CIFAR10 network comprises three convolutional layers with max pooling and ReLU activation functions. The outputs of the last convolutional layer are flattened and fed into a fully-connected feed-forward section of the network employing tanh activation functions (Appendix A.5). Due to the conceptual difficulties with quantizing functions with semi-infinite ranges we applied the quantization with 8 levels only to the last layers with tanh activation function, which are also the ones analyzed later. For 10 random weight initializations, the CIFAR10 network achieves an average accuracy of 99.90(4) % on the train and 68.9(7) % on the test set after 10^4 epochs of stochastic gradient descent training.

4.1 Representational complexity in small layers

For layers with up to five variables, the quintivariate PID can be computed in full. For the MNIST network with eight quantization levels, analyzing the mutual information of the hidden layers L_2, L_3 and L_4 with the ground-truth label allows to track the representational complexity both over training and through the successive layers (Figure 3.B). We find that both with increasing training epoch and layer index, the representational complexity C decreases.

This decrease in representational complexity appears to be a robust trend observable in networks independent of the encoding enforced on the output layer, chosen task and network architecture. While a neural network seems to approach the output complexity in the case of a one-hot output representation, for which $C_{\text{one-hot}} = 1$ (proven in Appendix A.4), the representational complexity of the hidden layers decreases below that of the

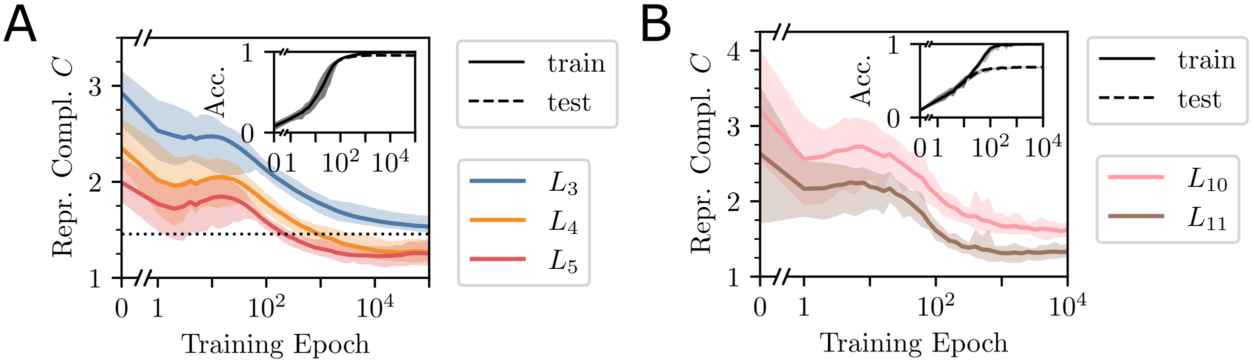

Figure 4: **The observed decrease in representational complexity appears to be a robust trend reproducible on different output encodings and on larger convolutional networks solving CIFAR10. A** The MNIST network with a binary output encoding shows a brief increase in representational complexity after about 10 epochs of training before decreasing. The representational complexity of the binary output layer for 10 equiprobable classes has been numerically determined to be $C = 1.46$ and is indicated by a dotted line. **B** The representational complexity of the small fully-connected layers of the CIFAR10 network shows a similar small increase in representational complexity in the beginning before converging to a low value close to the theoretical minimum of $C = 1$.

targeted output representation in the case of a binary label encoding (Figure 4.A). In the binary encoding case, however, an intermediate increase in representational complexity is observable, which might be attributable to an early restructuring of the representation.

Likewise, for the five-neuron layers L_{10} and L_{11} of the CIFAR10 network, one observes a plateau of the representational complexity until about epoch 10 which is followed by a subsequent decrease (Figure 4.B). Again, C is lower for the layer later in the network.

4.2 Representational complexity in larger layers

Typical production neural networks have layers which are much wider than five neurons (e.g., He et al., 2016; Krizhevsky et al., 2012). Since the compute required for a full PID for six or more source variables is prohibitive because of the rapidly increasing number of atoms, in order to be able to apply the tool of PID in general and representational complexity in particular to wider layers, one needs to devise procedures to reduce the number of random variables to analyze. In this section, we present two complementary approaches to make representational complexity applicable to moderately wider layers, namely subsampling and coarse-graining, and show the latter to be the more theoretically sound approach.

Subsampling A straightforward approach for reducing the number of random variables, which has been employed in previous works (e.g., Tax et al., 2017), is to *subsample* only $\hat{n}$ neurons from a layer to use as PID sources. By randomly selecting five neurons from the second layer of the MNIST network with four quantization levels, we again observe a decrease of the representational complexity of the hidden layer with respect to the label over the training phase (Figure 5.A, B), albeit with a larger amount of variability.

However, this approach suffers from fundamental conceptual flaws. By dissecting the mutual mutual information terms $I(T : \boldsymbol{S_a})$ of the target with only a subset of neurons $\boldsymbol{S_a}$, only atoms with a degree of synergy of less than or equal to $\hat{n}$ can be quantified, resulting in a potential underestimation of representational complexity. At the same time, pieces of information that appear to only be obtainable synergistically within one subset $\boldsymbol{S_a}$ of sources may very well be redundant with a single source $S_i \notin \boldsymbol{S_a}$, thus leading to potential overestimation of representational complexity. For these reasons, no bound on the true representational complexity can be established from subsampling and we find subsampling to be an unsuitable approach for overcoming the scaling difficulties of PID.

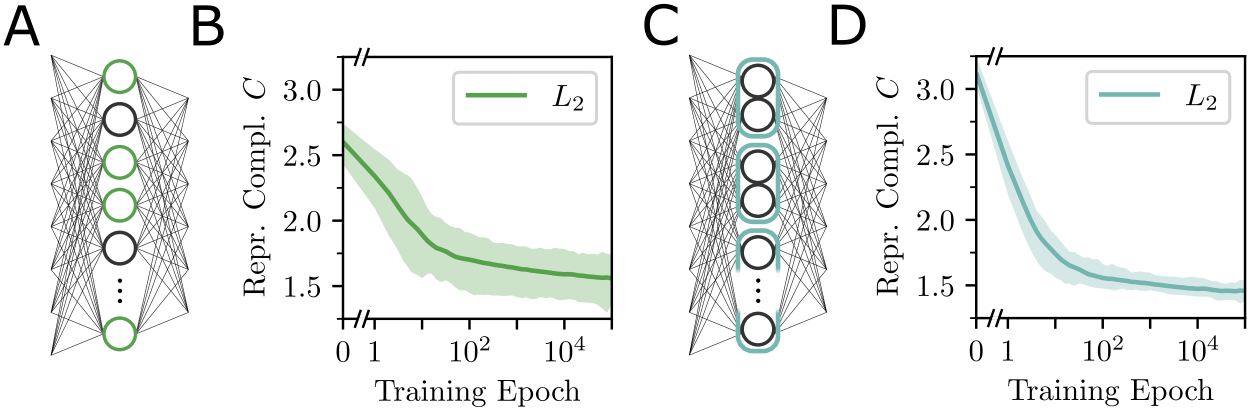

Figure 5: **Representational complexity of subsampled and coarse-grained neurons decreases over training in the MNIST network with four quantization levels.** **A** Five neurons are randomly selected from layer L_2 of the MNIST network to form the random variables for the subsampling analysis. **B** For 26 random choices of source variables each on 20 training runs, the subsampled representational complexity shows a decrease over the training phase, but with high variance. **C** Five coarse-grained random variables are constructed from pairs of neurons of the second hidden layer. **D** The coarse-grained representational complexity averaged over 20 training runs is seen to decrease with increasing training epoch.

Coarse-graining A complementary, more theoretically sound approach to reduce the number of variables is to combine multiple neurons, forming fewer higher-dimensional random variables; this procedure will be referred to as *coarse-graining.* In Appendix A.3, we prove that if d neurons S_i each are combined to random variables $\tilde{S}_j$, the true representational complexity of the layer is bounded from below by the coarse-grained representational complexity computed from $\tilde{\boldsymbol{S}} = \{\tilde{S}_1, \dots, \tilde{S}_{n/d}\}$, while being simultaneously bounded from above by d times this value, i.e.,

$$C(T : \tilde{\boldsymbol{S}}) \leq C(T : \boldsymbol{S}) \leq d\, C(T : \tilde{\boldsymbol{S}}). \tag{6}$$

In our example network with four quantization levels, the representational complexity computed from randomly assigned neuron pairs in the second hidden layer consisting of ten neurons, exhibits a decreasing pattern over training that is highly similar to that of the representational complexity computed with individual neurons as sources in layers L_3 to L_5 (Figure 5.C, D).

5 Discussion

In this work, we introduced representational complexity as a measure of sparsity of task-relevant information in neural networks. We first explained how a principled and meaningful application of information theory in neural networks is possible by using quantized activation values in both training and evaluation. Subsequently, we derived representational complexity from partial information decomposition and show it to be the theoretically sound answer to the question of how many neurons need to be observed simultaneously in order to access an average piece of information. For larger layers, we presented subsampling and coarse-graining procedures. We discussed issues with the former approach, while deriving bounds from results of the latter approach.

In small quantized deep neural networks, we find representational complexity to decrease both over training and through successive layers. We empirically find the reduction to be a robust result which can not only be observed when analyzing small layers neuron-wise, but also when using subsampling or coarse-graining on larger layers. Furthermore, we provide first evidence that the final values the representational complexity converges to do not depend on the representational complexity of the chosen output representation. We hypothesize that the dynamics of representational complexity in early stages of training might indicate an early restructuring of representations for the binary output encoding and the more complex CIFAR10 task.

Our results indicate some problems with previous approaches that apply PID by subsampling only pairs of sources (e.g. (Tax et al., 2017)). Since the representational complexity is high in the early stages of training, high-order interactions between neurons appear to play a major role. These, however, go unnoticed in pairwise approaches.

Limitations Scaling our approach to larger networks remains a challenge. To mitigate this problem, we introduced subsampling and course-graining procedures, which allow the application of representational complexity to moderately larger networks. However, while subsampling suffers from conceptual flaws, the proven attainable bounds on coarse graining become impractically loose for large networks. For typical production networks we suggest two approaches: Firstly, results found on small toy networks may be generalizable to larger networks, e.g., by inductive proofs, and secondly, estimation of representational complexity could become feasible by finding a way to compute it without computing all PID atoms beforehand. The latter can be achieved by employing a PID based on synergy instead of redundancy, for example by extending on ideas of Rosas et al. (2020).

Furthermore, our analysis methods are currently restricted to intrinsically discrete systems, as $I_\cap^{\mathrm{sx}}$ was originally defined for discrete variables only (Makkeh et al., 2021). However, in the meantime, a continuous generalization of $I_\cap^{\mathrm{sx}}$ has been proven to exist and to be measure-theoretically well-defined (Schick-Poland et al., 2021). Once an efficient estimator for this generalized measure is available, this will make it possible to analyze also continuous systems in which the total mutual information is inherently restricted to a finite value, e.g., by some form of noise in the system.

Conclusion and outlook We have here shown how to use the representational complexity to gain insight into the structure of the internal representations as an average across all source and target realizations. Due to the local nature of $I_\cap^{\mathrm{sx}}$, this analysis can also be further broken down into the representational complexity for individual target realizations, i.e., class labels. Such an analysis may reveal for example that some classes are linked to representations of high complexity while others are not, or that some classes are represented with low complexity earlier than others during training, while yet others fail to reach a low complexity. Complementary, a more detailed analysis could also be achieved by, instead of averaging over the different degrees of synergy, splitting up the total mutual information into “backbone atoms” (Rosas et al., 2020) which combine all atoms of the same degree of synergy m and investigating how they evolve over training individually.

Some theoretical properties of representational complexity have yet to be uncovered. For instance, a lower bound to C might be derived from the notion that closer to channel capacity, one is forced to represent some information in higher synergy terms.

Given the PID atoms, a whole suite of other interesting and easily interpretable measures can be devised. One enticing candidate is the average multiplicity of information, defined as $M = (1/I(T : \boldsymbol{S})) \sum_\alpha \Pi(\alpha)\,|\alpha|$. The quantity reflects the average number of times a piece of information is represented redundantly and thus appears to be a promising candidate to serve as a complementary summary statistic to representational complexity, which relates to the synergy of the information encoding.

In future research, one may also choose the PID source and target variables differently. While in this work we focused on analyzing how the information about the classification label is encoded in the network, a similar analysis for the information of the hidden layers about the whole input samples might reveal differences in the representation of task-relevant and task-irrelevant information.

More generally, we promote representational complexity as a principled novel tool for general complex systems in which a group of equivalent variables jointly holds information about a target variable. New possible applications include both other artificial network architectures such as recurrent networks, but also biological or ecological systems. Being derived from first principles in information theory and partial information decomposition, representational complexity provides a clear and intuitive interpretation and the suggested subsampling and coarse-graining procedures make it applicable to a wide variety of questions.

References

Yann LeCun, Yoshua Bengio, and Geoffrey Hinton. Deep learning. *nature*, 521(7553):436–444, 2015.

Md Zahangir Alom, Tarek M Taha, Chris Yakopcic, Stefan Westberg, Paheding Sidike, Mst Shamima Nasrin, Mahmudul Hasan, Brian C Van Essen, Abdul AS Awwal, and Vijayan K Asari. A state-of-the-art survey on deep learning theory and architectures. *Electronics*, 8(3):292, 2019.

Wojciech Samek, Thomas Wiegand, and Klaus-Robert Müller. Explainable artificial intelligence: Understanding, visualizing and interpreting deep learning models. *arXiv preprint arXiv:1708.08296*, 2017.

Yixuan Li, Jason Yosinski, Jeff Clune, Hod Lipson, and John Hopcroft. Convergent learning: Do different neural networks learn the same representations? In *Feature Extraction: Modern Questions and Challenges*, pages 196–212. PMLR, 2015.

Yoshua Bengio, Aaron Courville, and Pascal Vincent. Representation learning: A review and new perspectives. *IEEE transactions on pattern analysis and machine intelligence*, 35(8):1798–1828, 2013.

Dario Amodei, Chris Olah, Jacob Steinhardt, Paul Christiano, John Schulman, and Dan Mané. Concrete problems in ai safety. *arXiv preprint arXiv:1606.06565*, 2016.

Kevin Eykholt, Ivan Evtimov, Earlence Fernandes, Bo Li, Amir Rahmati, Chaowei Xiao, Atul Prakash, Tadayoshi Kohno, and Dawn Song. Robust physical-world attacks on deep learning visual classification. In *Proceedings of the IEEE conference on computer vision and pattern recognition*, pages 1625–1634, 2018.

Claude Elwood Shannon. A mathematical theory of communication. *The Bell system technical journal*, 27 (3):379–423, 1948.

Naftali Tishby and Noga Zaslavsky. Deep learning and the information bottleneck principle. In *2015 IEEE Information Theory Workshop (ITW)*, pages 1–5. IEEE, 2015.

Andrew M Saxe, Yamini Bansal, Joel Dapello, Madhu Advani, Artemy Kolchinsky, Brendan D Tracey, and David D Cox. On the information bottleneck theory of deep learning. *Journal of Statistical Mechanics: Theory and Experiment*, 2019(12):124020, 2019.

Ziv Goldfeld, Ewout van den Berg, Kristjan Greenewald, Igor Melnyk, Nam Nguyen, Brian Kingsbury, and Yury Polyanskiy. Estimating information flow in deep neural networks. *International Conference on Machine Learning*, 2019.

Ravid Shwartz-Ziv and Naftali Tishby. Opening the black box of deep neural networks via information. *arXiv preprint arXiv:1703.00810*, 2017.

Paul L Williams and Randall D Beer. Nonnegative decomposition of multivariate information. *arXiv preprint arXiv:1004.2515*, 2010.

Aaron J Gutknecht, Michael Wibral, and Abdullah Makkeh. Bits and pieces: Understanding information decomposition from part-whole relationships and formal logic. *Proceedings of the Royal Society A*, 477 (2251):20210110, 2021.

Bernhard C Geiger. On information plane analyses of neural network classifiers–a review. *IEEE Transactions on Neural Networks and Learning Systems*, 2021.

Suyog Gupta, Ankur Agrawal, Kailash Gopalakrishnan, and Pritish Narayanan. Deep learning with limited numerical precision. In *International conference on machine learning*, pages 1737–1746. PMLR, 2015.

Itay Hubara, Matthieu Courbariaux, Daniel Soudry, Ran El-Yaniv, and Yoshua Bengio. Quantized neural networks: Training neural networks with low precision weights and activations. *The Journal of Machine Learning Research*, 18(1):6869–6898, 2017.

Michael Wibral, Conor Finn, Patricia Wollstadt, Joseph T Lizier, and Viola Priesemann. Quantifying information modification in developing neural networks via partial information decomposition. *Entropy*, 19 (9):494, 2017.

Shujian Yu, Kristoffer Wickstrøm, Robert Jenssen, and Jose C Principe. Understanding convolutional neural networks with information theory: An initial exploration. *IEEE transactions on neural networks and learning systems*, 32(1):435–442, 2020.

Tycho Tax, Pedro AM Mediano, and Murray Shanahan. The partial information decomposition of generative neural network models. *Entropy*, 19(9):474, 2017.

Kyle Reing, Greg Ver Steeg, and Aram Galstyan. Discovering higher-order interactions through neural information decomposition. *Entropy*, 23(1):79, 2021.

Hyunjik Kim and Andriy Mnih. Disentangling by factorising. In *International Conference on Machine Learning*, pages 2649–2658. PMLR, 2018.

Ricky TQ Chen, Xuechen Li, Roger B Grosse, and David K Duvenaud. Isolating sources of disentanglement in variational autoencoders. *Advances in neural information processing systems*, 31, 2018.

Seiya Tokui and Issei Sato. Disentanglement analysis with partial information decomposition. *arXiv preprint arXiv:2108.13753*, 2021.

Yilun Xu, Shengjia Zhao, Jiaming Song, Russell Stewart, and Stefano Ermon. A theory of usable information under computational constraints. In *International Conference on Learning Representations*, 2019.

Michael Kleinman, Alessandro Achille, Daksh Idnani, and Jonathan Kao. Usable information and evolution of optimal representations during training. In *International Conference on Learning Representations*, 2020.

Guillaume Alain and Yoshua Bengio. Understanding intermediate layers using linear classifier probes. *International Conference on Learning Representations*, 2017.

Alessio Ansuini, Alessandro Laio, Jakob H Macke, and Davide Zoccolan. Intrinsic dimension of data representations in deep neural networks. *Advances in Neural Information Processing Systems*, 32, 2019.

Ari Morcos, Maithra Raghu, and Samy Bengio. Insights on representational similarity in neural networks with canonical correlation. *Advances in Neural Information Processing Systems*, 31, 2018.

Simon Kornblith, Mohammad Norouzi, Honglak Lee, and Geoffrey Hinton. Similarity of neural network representations revisited. In *International Conference on Machine Learning*, pages 3519–3529. PMLR, 2019.

Yiding Jiang, Behnam Neyshabur, Hossein Mobahi, Dilip Krishnan, and Samy Bengio. Fantastic generalization measures and where to find them. In *International Conference on Learning Representations*, 2019.

Doug Wiedemann. A computation of the eighth dedekind number. *Order*, 8(1):5–6, 1991.

Jason Crampton and George Loizou. Two partial orders on the set of antichains, 2000.

Jason Crampton and George Loizou. The completion of a poset in a lattice of antichains. *International Mathematical Journal*, 1(3):223–238, 2001.

Gian-Carlo Rota. On the foundations of combinatorial theory i. theory of möbius functions. *Zeitschrift für Wahrscheinlichkeitstheorie und verwandte Gebiete*, 2(4):340–368, 1964.

Joseph T Lizier, Nils Bertschinger, Jürgen Jost, and Michael Wibral. Information decomposition of target effects from multi-source interactions: Perspectives on previous, current and future work. *Entropy*, 20(4): 307, 2018.

Nils Bertschinger, Johannes Rauh, Eckehard Olbrich, Jürgen Jost, and Nihat Ay. Quantifying unique information. *Entropy*, 16(4):2161–2183, 2014.

Robin AA Ince. Measuring multivariate redundant information with pointwise common change in surprisal. *Entropy*, 19(7):318, 2017.

Conor Finn and Joseph T Lizier. Pointwise partial information decomposition using the specificity and ambiguity lattices. *Entropy*, 20(4):297, 2018.

Abdullah Makkeh, Aaron J Gutknecht, and Michael Wibral. Introducing a differentiable measure of pointwise shared information. *Physical Review E*, 103(3):032149, 2021.

Bruno A Olshausen and David J Field. Sparse coding of sensory inputs. *Current opinion in neurobiology*, 14 (4):481–487, 2004.

Yann LeCun, Léon Bottou, Yoshua Bengio, and Patrick Haffner. Gradient-based learning applied to document recognition. *Proceedings of the IEEE*, 86(11):2278–2324, 1998.

Alex Krizhevsky. Learning multiple layers of features from tiny images, 2009.

Kaiming He, Xiangyu Zhang, Shaoqing Ren, and Jian Sun. Deep residual learning for image recognition. In *Proceedings of the IEEE conference on computer vision and pattern recognition*, pages 770–778, 2016.

Alex Krizhevsky, Ilya Sutskever, and Geoffrey E Hinton. Imagenet classification with deep convolutional neural networks. *Advances in neural information processing systems*, 25, 2012.

Fernando E Rosas, Pedro AM Mediano, Borzoo Rassouli, and Adam B Barrett. An operational information decomposition via synergistic disclosure. *Journal of Physics A: Mathematical and Theoretical*, 53(48): 485001, 2020.

Kyle Schick-Poland, Abdullah Makkeh, Aaron J Gutknecht, Patricia Wollstadt, Anja Sturm, and Michael Wibral. A partial information decomposition for discrete and continuous variables. *arXiv preprint arXiv:2106.12393*, 2021.

Thomas M Cover and Joy A Thomas. Elements of information theory 2nd edition (wiley series in telecommunications and signal processing). *Acessado em*, 2006.

Chhavi Yadav and Léon Bottou. Cold case: The lost mnist digits. *Advances in neural information processing systems*, 32, 2019.

A Appendix

A.1 Equivalence between parthood distributions and antichains

An information atom Π can be equivalently referenced by either its parthood distribution Φ as $\Pi(T : \boldsymbol{S}_\Phi)$ or its corresponding antichain α as $\Pi(T : \boldsymbol{S}_\alpha)$. This equivalence is given by the facts that (i) the parthood distributions $\Phi : \mathcal{P}(\{1, \dots, n\}) \to \{0, 1\}$ are *monotonic*, i.e., they fulfill the relation $\boldsymbol{a} \subseteq \boldsymbol{b} \Rightarrow \Phi(\boldsymbol{a}) \leq \Phi(\boldsymbol{b})$, and (ii) antichains are succinct representations of such monotonic boolean functions. To gain a deeper insight into the equivalent descriptions of the atoms, we will thus address these two points one by one in the following.

First, note that the monotonicity of the parthood distributions necessarily follows from the properties of mutual information: The mutual information $I(T : \boldsymbol{S}_{\boldsymbol{a}})$ between the target T and a subset of sources $\boldsymbol{S}_{\boldsymbol{a}}$ is contained in the mutual information $I(T : \boldsymbol{S}_{\boldsymbol{b}})$ whenever $\boldsymbol{b}$ is a superset of $\boldsymbol{a}$. This fact is a result of the chain rule of mutual information and the non-negativity of (conditional) mutual information (Cover and Thomas, 2006) $I(T : \boldsymbol{S}_{\boldsymbol{b}}) = I(T : \boldsymbol{S}_{\boldsymbol{a}}, \boldsymbol{S}_{\boldsymbol{b} \setminus \boldsymbol{a}}) = I(T : \boldsymbol{S}_{\boldsymbol{a}}) + I(T : \boldsymbol{S}_{\boldsymbol{b} \setminus \boldsymbol{a}} | \boldsymbol{S}_{\boldsymbol{a}}) \geq I(T : \boldsymbol{S}_{\boldsymbol{a}})$ and formalizes the intuitive fact that the predictability of the target can only increase when additional source variables are observed. This means that if an atom Π is part of the mutual information $I(T : \boldsymbol{S}_{\boldsymbol{a}})$, i.e., $\Phi(\boldsymbol{a}) = 1$, it also has to be part of $I(T : \boldsymbol{S}_{\boldsymbol{b}})$, i.e., $\Phi(\boldsymbol{b}) = 1$ whenever $\boldsymbol{a} \subseteq \boldsymbol{b}$, which is exactly the property of monotonicity: $\boldsymbol{a} \subseteq \boldsymbol{b} \Rightarrow \Phi(\boldsymbol{a}) \leq \Phi(\boldsymbol{b})$.

Second, note that any boolean function is uniquely defined by the set of inputs $f^{-1}[\{1\}] := \{\boldsymbol{a} \in \mathcal{P}(\{1, \dots, n\}) \mid f(\boldsymbol{a}) = 1\}$ that are mapped to "1". Given the constraint of monotonicity, this representation can be compressed even further: Any sets which are supersets of others need not be recorded, as these are forced to map to "1" by monotonicity. Thus, a monotonic boolean function can be represented by $\alpha \subseteq f^{-1}[\{1\}]$, constructed by removing all sets in $f^{-1}[\{1\}]$ which are supersets of others. The resulting set of sets α then contains only sets which are incomparable given the partial order of set inclusion, which are referred to in the literature as "antichains" (Williams and Beer, 2010).

Therefore, each PID $I(T : \boldsymbol{S}_\Phi)$ atom identified with a parthood distribution Φ can be represented by the antichain representation of Φ, which provides an equivalent labelling of the atom as $I(T : \boldsymbol{S}_\alpha)$.

A.2 The lattice structure of PID

Similar to the ordering of the mutual information terms described before, the general redundancies $I_\cap(T : \boldsymbol{S}_\Phi)$ also have a canonical ordering. Here, the intuitive idea is that a redundancy $I_\cap(T : \boldsymbol{S}_\Phi)$ is contained in another redundancy $I_\cap(T : \boldsymbol{S}_\Psi)$ if the latter is part of all the mutual information terms $I(T : S_{\boldsymbol{a}})$ that the first is part of, which makes any part of information contained in $I_\cap(T : \boldsymbol{S}_\Phi)$ also contained in $I_\cap(T : \boldsymbol{S}_\Psi)$. In terms of parthood distributions, this condition is given by (Gutknecht et al., 2021)

$$\Phi \sqsubseteq \Psi \Leftrightarrow (\Phi(\boldsymbol{a}) = 1 \to \Psi(\boldsymbol{a}) = 1 \text{ for any } \boldsymbol{a} \subseteq \{1, \dots, n\}). \tag{7}$$

Using the equivalence established in Appendix A.1, this partial order can be expressed in terms of antichains as (Williams and Beer, 2010)

$$\alpha \preceq \beta \Leftrightarrow \forall \boldsymbol{b} \in \beta \; \exists \boldsymbol{a} \in \alpha : a \subseteq b. \tag{8}$$

This partial ordering defines the algebraic structure of the "Redundancy Lattice". Interpreting the redundancies $I_\cap$ as partial sums on this lattice, as described in Equation (3), the atoms can be computed from the redundancies by means of a Moebius Inversion (Williams and Beer, 2010).

A.3 Proof of bounds on representational complexity by coarse-graining

To make representational complexity applicable to settings with more source random variables, we propose coarse-graining, i.e., combining source variables to form fewer, but higher dimensional, "super variables", as a suitable procedure. As a first step, we clarify how the new coarse-grained variables are constructed from the original variables using a *coarse-grain mapping.*

Definition A.1 (Coarse-Grain mapping)**.** For $n, \tilde{n} \in \mathbb{N}_{>0}$ and $\tilde{n} < n$, an n-to-$\tilde{n}$ coarse-grain mapping $f : \{1, \dots, n\} \to \{1, \dots, \tilde{n}\}$ is a surjective function that maps variable indices to fewer coarse-grained variable indices.

We write the pre-image of the coarse-grain mapping for subsets of coarse-grained source indices $\tilde{\boldsymbol{a}} \subseteq \{1, \dots, \tilde{n}\}$ as $f^{-1}[\tilde{\boldsymbol{a}}] = \{i \in \{1, \dots, n\} | f(i) \in \tilde{\boldsymbol{a}}\}$.

Furthermore, we write sets of random variables indexed by the set of indices $\boldsymbol{a} \in \mathcal{P}(\{1, \dots, n\})$ as $\boldsymbol{S}_{\boldsymbol{a}} = \{S_i | i \in \boldsymbol{a}\}$ and finally sets of sets of random variables indexed by sets of sets of indices $\alpha \in \mathcal{P}(\mathcal{P}(\{1, \dots, n\}))$ as $\boldsymbol{S}_\alpha = \{\boldsymbol{S}_{\boldsymbol{a}} | \boldsymbol{a} \in \alpha\}$.

Using this notion of a coarse-grain mapping, we can define what a coarse-grained random variables is.

Definition A.2 (Coarse-Grained Random Variable)**.** Given a vector-valued random variable $\boldsymbol{S} = (S_1, \dots, S_n)$ and an n-to-$\tilde{n}$ coarse-grain mapping f, the coarse-grained vector-valued random variable $\tilde{\boldsymbol{S}}$ is defined as $\tilde{\boldsymbol{S}} = (\tilde{\boldsymbol{S}}_1, \dots, \tilde{\boldsymbol{S}}_{\tilde{n}})$, where the elements $\tilde{\boldsymbol{S}}_i = \boldsymbol{S}_{f^{-1}[\{i\}]} = \{S_k | f(k) = i\}$ are themselves vector-valued random variables, called coarse-grained variables, partitioning the n original variables into $\tilde{n}$ variables.

Example A.1. Given four source variables $\boldsymbol{S} = (S_1, S_2, S_3, S_4)$, the mapping

$$f : \{1, 2, 3, 4\} \to \{1, 2\},\ i \mapsto \begin{cases} 1,\ i \in \{1, 2\} \\ 2,\ i \in \{3, 4\} \end{cases}$$

defines the two coarse-grained random variables $\tilde{\boldsymbol{S}}_1 = (S_1, S_2)$ and $\tilde{\boldsymbol{S}}_2 = (S_3, S_4)$.

In general, a coarse-grain mapping can produce coarse-grained variables consisting of different numbers of original variables. An important special case, however, is that of the *uniform coarse-grain mapping*, which always maps d source variables to one d-dimensional "super-variable".

Definition A.3 (Uniform coarse-grain mapping)**.** A uniform coarse-grain mapping of order $d \in \mathbb{N}_{>0}$ such that $d|n$ is given by $f : \{1, \dots, n\} \to \{1, \dots, n/d\},\ i \mapsto \lfloor (i-1)/d \rfloor + 1$, where $\lfloor \cdot \rfloor$ refers to rounding down to the nearest integer.

Having defined the coarse-grained variables $\tilde{\boldsymbol{S}}$, the next question that arises is how the PID atoms of the original variables can be combined to form the coarse-grained PID atoms of $\tilde{\boldsymbol{S}}$.

Theorem A.1 (Coarse-graining of PID atoms)**.** *The PID atoms* $\Pi(T : \tilde{\boldsymbol{S}}_{\tilde{\Phi}})$ *of the coarse-grained source variable* $\tilde{\boldsymbol{S}}$ *are composed of the PID atoms* $\Pi(T : \boldsymbol{S}_\Phi)$ *of the original sources* $\boldsymbol{S}$ *as*

$$\Pi\left(T : \tilde{\boldsymbol{S}}_{\tilde{\Phi}}\right) = \sum_{\Phi : \Phi \circ f^{-1} = \tilde{\Phi}} \Pi\left(T : \boldsymbol{S}_\Phi\right). \tag{9}$$

Proof. A PID atom $\Pi\left(T : \boldsymbol{S}_\Phi\right)$ is a part of the coarse-grained PID atom $\Pi\left(T : \tilde{\boldsymbol{S}}_{\tilde{\Phi}}\right)$ exactly if it contributes to the same mutual information terms $I\left(T : \tilde{\boldsymbol{S}}_{\tilde{\boldsymbol{a}}}\right)$ with the coarse-grained variables $\tilde{\boldsymbol{S}}_{\tilde{\boldsymbol{a}}}$. Since the identity

$$I\left(T : \tilde{\boldsymbol{S}}_{\tilde{\boldsymbol{a}}}\right) = I\left(T : \boldsymbol{S}_{f^{-1}[\tilde{\boldsymbol{a}}]}\right)$$

follows readily from the definition of the coarse-grained variables, we find that if $\Pi\left(T : \boldsymbol{S}_\Phi\right)$ is part of $I\left(T : \boldsymbol{S}_{f^{-1}[\tilde{\boldsymbol{a}}]}\right)$, i.e., $\Phi(f^{-1}[\tilde{\boldsymbol{a}}]) = 1$, it is also part of $I\left(T : \tilde{\boldsymbol{S}}_{\tilde{\boldsymbol{a}}}\right)$ in the coarse-grained picture, and vice-versa. Thus, the parthood relations of $\Pi\left(T : \boldsymbol{S}_\Phi\right)$ with regards to the coarse-grained variables are captured by the parthood distribution $\tilde{\Phi} = \Phi \circ f^{-1}$, which leads to the conclusion that it must be part of the coarse-grained atom $\Pi\left(T : \tilde{\boldsymbol{S}}_{\tilde{\Phi}}\right)$. The coarse-grained atoms must now be the sums of all original atoms which contribute to the same coarse-grained mutual information terms; thus the theorem follows.

□

This coarse-grained PID naturally gives rise to both a lower and an upper bound on the representational complexity of the original variables. As a first step, we show how representational complexity can be equally computed from the parthood distribution Φ of an atom.

Lemma A.1 (Computing the degree of synergy from a parthood distribution)**.** *The degree of synergy of the atom indexed by the parthood distribution* Φ *is given by* $m(\Phi) = \min_{\Phi(\boldsymbol{a})=1} |\boldsymbol{a}|$.

Proof. The parthood distribution Φ corresponding to an antichain α is the boolean function that maps all $\boldsymbol{a} \in \alpha$ and all supersets thereof to one. This means, in addition to all sets $\boldsymbol{a} \in \alpha$, that $\Phi^{-1}[\{1\}]$, the fibre of 1 under Φ, contains only sets $\boldsymbol{a}' \supset \boldsymbol{a}$, for which $|\boldsymbol{a}'| > |\boldsymbol{a}|$ and which thus have no influence on the minimum cardinality of sets:

$$m(\alpha) := \min_{\boldsymbol{a}\in\alpha} |\boldsymbol{a}| = \min_{\boldsymbol{a}\in\Phi^{-1}[\{1\}]} |\boldsymbol{a}| = \min_{\Phi(\boldsymbol{a})=1} |\boldsymbol{a}| =: m(\Phi)\,. \tag{10}$$

□

The next step in our quest to prove bounds on the representational complexity is to prove bounds on the degree of synergy m.

Lemma A.2. *Let* Φ *and* $\tilde{\Phi}$ *refer to the parthood distributions of an atom and a coarse-grained atom, respectively. If* $\Pi(T : \boldsymbol{S}_\Phi)$ *is part of* $\Pi(T : \tilde{\boldsymbol{S}}_{\tilde{\Phi}})$*, then the degree of synergy* $m(\Phi)$ *is constrained by the degree of synergy* $m(\tilde{\Phi})$ *as* $m(\tilde{\Phi}) \leq m(\Phi) \leq d\, m(\tilde{\Phi})$*, where the upper bound holds for a uniform coarse-graining of order* d*.*

Proof. Let the atom $\Pi(T : \boldsymbol{S}_\Phi)$ be part of the coarse-grained atom $\Pi(T : \tilde{\boldsymbol{S}}_{\tilde{\Phi}})$. It follows from Equation (9) that $\tilde{\Phi} = \Phi \circ f^{-1}$ and therefore

$$m(\tilde{\Phi}) = \min_{\tilde{\Phi}(\tilde{\boldsymbol{a}})=1} |\tilde{\boldsymbol{a}}| = \min_{\Phi\circ f^{-1}(\tilde{\boldsymbol{a}})=1} |\tilde{\boldsymbol{a}}| = \min_{\Phi(\boldsymbol{a})=1} |f(\boldsymbol{a})| \leq \min_{\Phi(\boldsymbol{a})=1} |\boldsymbol{a}| = m(\Phi)\,,$$

where the fact that $|f(\boldsymbol{a})| \leq |\boldsymbol{a}|$ has been used. Note similarly that for a uniform coarse-graining of order d, $d|f(\boldsymbol{a})| \geq |\boldsymbol{a}|$ holds, hence one finds a lower bound to $m(\tilde{\Phi})$ as

$$m(\tilde{\Phi}) = \min_{\Phi(\boldsymbol{a})=1} |f(\boldsymbol{a})| \geq \frac{1}{d} \min_{\Phi(\boldsymbol{a})=1} |\boldsymbol{a}| = \frac{1}{d} m(\Phi)\,.$$

□

From the bounds on the synergistic degree, the bounds on the representational complexity - which is a weighted average of synergistic degrees - are straightforward to derive.

Theorem A.2. *The representational complexity of a vector of sources* $\boldsymbol{S} = (S_1, \ldots, S_n)$ *with respect to some target* T *is bounded from below by the representational complexity of any coarse-graining* $\tilde{\boldsymbol{S}}$

$$C(T : \tilde{\boldsymbol{S}}) \leq C(T : \boldsymbol{S})\,. \tag{11}$$

Proof.

$$\begin{aligned}
C(T:\tilde{\boldsymbol{S}}) &= \frac{1}{I(T:\tilde{\boldsymbol{S}})}\sum_{\tilde{\Phi}}\Pi(T:\tilde{\boldsymbol{S}}_{\tilde{\Phi}})\,m(\tilde{\Phi}) \\
&= \frac{1}{I(T:\tilde{\boldsymbol{S}})}\sum_{\tilde{\Phi}}\left(\sum_{\Phi:\Phi\circ f^{-1}=\tilde{\Phi}}\Pi\left(T:\boldsymbol{S}_{\Phi}\right)\right)\,m(\tilde{\Phi}) && \text{(Theorem A.1)} \\
&\leq \frac{1}{I(T:\tilde{\boldsymbol{S}})}\sum_{\tilde{\Phi}}\sum_{\Phi:\Phi\circ f^{-1}=\tilde{\Phi}}\Pi\left(T:\boldsymbol{S}_{\Phi}\right)\,m(\Phi) && \text{(Lemma A.2)} \\
&= \frac{1}{I(T:\boldsymbol{S})}\sum_{\Phi}\Pi\left(T:\boldsymbol{S}_{\Phi}\right)\,m(\Phi) \\
&= C(T:\boldsymbol{S})\,.
\end{aligned}$$

□

Theorem A.3. *The representational complexity of a vector of sources $\boldsymbol{S}=(S_1,\dots,S_n)$ with respect to some target T is bounded from above by d times the representational complexity of a uniform coarse-graining of order d*

$$C(T:\boldsymbol{S}) \leq d\,C(T:\tilde{\boldsymbol{S}})\,. \tag{12}$$

Proof.

$$\begin{aligned}
C(T:\tilde{\boldsymbol{S}}) &= \frac{1}{I(T:\tilde{\boldsymbol{S}})}\sum_{\tilde{\Phi}}\Pi(T:\tilde{\boldsymbol{S}}_{\tilde{\Phi}})\,m(\tilde{\Phi}) \\
&= \frac{1}{I(T:\tilde{\boldsymbol{S}})}\sum_{\tilde{\Phi}}\left(\sum_{\Phi:\Phi\circ f^{-1}=\tilde{\Phi}}\Pi\left(T:\boldsymbol{S}_{\Phi}\right)\right)\,m(\tilde{\Phi}) && \text{(Theorem A.1)} \\
&\geq \frac{1}{I(T:\tilde{\boldsymbol{S}})}\sum_{\tilde{\Phi}}\sum_{\Phi:\Phi\circ f^{-1}=\tilde{\Phi}}\Pi\left(T:\boldsymbol{S}_{\Phi}\right)\,m(\Phi)/d && \text{(Lemma A.2)} \\
&= \frac{1}{d\,I(T:\boldsymbol{S})}\sum_{\Phi}\Pi\left(T:\boldsymbol{S}_{\Phi}\right)\,m(\Phi) \\
&= \frac{1}{d}C(T:\boldsymbol{S})\,.
\end{aligned}$$

□

A.4 Proof of representational complexity of one-hot encoding

In DNNs solving a classification task, the output labels are typically encoded in a “One-Hot Encoding”, in which there are as many neurons as classes with only the neuron corresponding to the correct class being one while all others are zero. Here we prove that all such encodings have a representational complexity of $C=1$.

Definition A.4 (One-hot encoding)**.** The one-hot encoding $\vec{Y}$ of a categorical variable Y with finite ordered alphabet $A_Y=(y_1,y_2,\dots,y_n)$ is the image of the bijective mapping

$$\vec{\cdot}: A_Y \to A_{\vec{Y}} \subset \{0,1\}^n, y \mapsto \vec{y} = (\delta_{y,y_j})_j = (0,\dots,\underbrace{0}_{j-1},\underbrace{1}_{j},\underbrace{0}_{j+1},\dots,0)\,,$$

where δ_{y,y_j} is the Kronecker Delta.

In what follows, we recall the concepts of local mutual information i, local $I_\cap^{\mathrm{sx}}$ redundancy $i_\cap^{\mathrm{sx}}$, and its additive decomposition into local informative redundancy $i_\cap^{\mathrm{sx}+}$ and local misinformative redundancy $i_\cap^{\mathrm{sx}-}$. These information functionals are needed in proving that any one-hot encoding has a representational complexity equals to one.

Definition A.5 (Local information and their informative and misinformative parts)**.** Let T be the target variable and $\boldsymbol{S}$ be the set of sources. Then, we have the following:

- The mutual information $I(T : \boldsymbol{S})$ is, in fact, the expected value of the local mutual information $i(t : \boldsymbol{s})$ as follows:
$$I(T : \boldsymbol{S}) := \sum_{t,\boldsymbol{s}} \mathbb{P}(\mathfrak{t} \cap \boldsymbol{\mathfrak{s}}) \log_2 \frac{\mathbb{P}\left(\mathfrak{t} \cap \boldsymbol{\mathfrak{s}}\right)}{\mathbb{P}\left(\mathfrak{t}\right) \mathbb{P}\left(\boldsymbol{\mathfrak{s}}\right)} = \mathbb{E}_{t,\boldsymbol{s}}\left[i(t : \boldsymbol{s})\right] .$$

- The local mutual information $i(t : \boldsymbol{s})$ can take negative values and so it is decomposed into nonnegative informative $i^+(t : \boldsymbol{s})$ and misinformative $i^-(t : \boldsymbol{s})$ parts as follows:
$$\begin{aligned} i^+(t : \boldsymbol{s}) &:= \log_2 \frac{1}{\mathbb{P}\left(\boldsymbol{\mathfrak{s}}\right)} = \log_2 \frac{1}{p_{\boldsymbol{S}}(\boldsymbol{s})} , \\ i^-(t : \boldsymbol{s}) &:= \log_2 \frac{\mathbb{P}\left(\mathfrak{t}\right)}{\mathbb{P}\left(\mathfrak{t} \cap \boldsymbol{\mathfrak{s}}\right)} = \log_2 \frac{1}{p_{\boldsymbol{S}|T}(\boldsymbol{s} \mid t)} . \end{aligned}$$

- The $I_\cap^{\mathrm{sx}}$ redundancy $I_\cap^{\mathrm{sx}}(T : \boldsymbol{S}_\alpha)$ is in its turn the expected value of the local redundant information $i^{\mathrm{sx}}(t : \boldsymbol{s}_\alpha)$ as follows:
$$I_\cap^{\mathrm{sx}}(T : \boldsymbol{S}_\alpha) = \sum_{t,\boldsymbol{s}} \mathbb{P}(\mathfrak{t} \cap \boldsymbol{\mathfrak{s}}) \log_2 \frac{\mathbb{P}\left(\mathfrak{t}\right) - \mathbb{P}\left(\mathfrak{t} \cap \bigcap_{\boldsymbol{a} \in \alpha} \bar{\boldsymbol{\mathfrak{s}}}_{\boldsymbol{a}}\right)}{\mathbb{P}\left(\mathfrak{t}\right)\left[1 - \mathbb{P}\left(\bigcap_{\boldsymbol{a} \in \alpha} \bar{\boldsymbol{\mathfrak{s}}}_{\boldsymbol{a}}\right)\right]} = \mathbb{E}_{t,\boldsymbol{s}}\left[i_\cap^{\mathrm{sx}}(t : \boldsymbol{s}_\alpha)\right] .$$

- The local $I_\cap^{\mathrm{sx}}$ redundancy $i_\cap^{\mathrm{sx}}(t : \boldsymbol{s}_\alpha)$ can also take negative values and so it is decomposed into nonnegative informative $i_\cap^{\mathrm{sx}+}(t : \boldsymbol{s}_\alpha)$ and misinformative $i_\cap^{\mathrm{sx}-}(t : \boldsymbol{s}_\alpha)$ parts as follows:
$$\begin{aligned} i_\cap^{\mathrm{sx}+}(t : \boldsymbol{s}_\alpha) &:= \log_2 \frac{1}{1 - \mathbb{P}\left(\bigcap_{\boldsymbol{a} \in \alpha} \bar{\boldsymbol{\mathfrak{s}}}_{\boldsymbol{a}}\right)} = \log_2 \frac{1}{p_{\boldsymbol{S}_\alpha}(\boldsymbol{s}_\alpha)} , \\ i_\cap^{\mathrm{sx}-}(t : \boldsymbol{s}_\alpha) &:= \log_2 \frac{\mathbb{P}\left(\mathfrak{t}\right)}{\mathbb{P}\left(\mathfrak{t}\right) - \mathbb{P}\left(\mathfrak{t} \cap \bigcap_{\boldsymbol{a} \in \alpha} \bar{\boldsymbol{\mathfrak{s}}}_{\boldsymbol{a}}\right)} = \log_2 \frac{1}{p_{\boldsymbol{S}_\alpha|T}(\boldsymbol{s}_\alpha \mid t)} . \end{aligned}$$

Proposition A.1. *The misinformative part of the redundancy $I_\cap^{\mathrm{sx}-}(T : \boldsymbol{S}_\alpha)$ vanishes if there exists a mapping $f : T \to \boldsymbol{S}$ from the target to the sources.*

Proof. If there exists a function $f : T \to \boldsymbol{S}$, all conditional probabilities of the form $p_{\boldsymbol{S}_\alpha|T}(\boldsymbol{s}_\alpha \mid t) = p_{\boldsymbol{S}_\alpha|T}((\boldsymbol{s}_{\boldsymbol{a}_{11}} \cap \boldsymbol{s}_{\boldsymbol{a}_{12}} \cap \dots) \cup \cdots \mid t)$ are equal to either one or zero. Thus, $I_\cap^{\mathrm{sx}-}(T : \boldsymbol{S}_\alpha) = -\sum_{\boldsymbol{s},t} p_{\boldsymbol{S},T}(\boldsymbol{s}, t) \log_2 p_{\boldsymbol{S}_\alpha|T}(\boldsymbol{s}_\alpha \mid t) = 0$ for any α. □

To uniquely determine the label from a one-hot representation, it is sufficient to observe the one neuron that is equal to one. However, one gets the same information by observing all neurons which are equal to zero, since, by exclusion, the last one then has to be one. Let $\alpha_j := \{\{j\}\{1, ..., j-1, j+1, ..., n\}\}$ be the antichain describing the redundant information between the j-th source and the rest of the sources taken together. Further, let $I(Y : \vec{Y})$ describe the mutual information between a random variable Y and its one-hot representation, which is trivially equal to its entropy $H(Y)$ due to the construction of $\vec{Y}$.

Lemma A.3. *The size of the local $I_\cap^{\mathrm{sx}}$ redundancy $i_\cap^{\mathrm{sx}}(y_j : \vec{y}_{\alpha_j})$ is $-\log_2 p_Y(y)$.*

Proof. Since the one-hot representation is a bijective function of the variable, Proposition A.1 implies that the misinformative part of the redundancy vanishes. The local $I_\cap^{\mathrm{sx}}$ redundancy in question then amounts to $i_\cap^{\mathrm{sx}}(y_j : \vec{y}_{\alpha_j}) = i_\cap^{\mathrm{sx}+}(y_j : \vec{y}_{\alpha_j}) = -\log_2 p_Y(y_j \cup (y_1 \cap \cdots \cap y_{j-1} \cap y_{j+1} \cap \cdots \cap y_n)) = -\log_2 p_Y(y_j \cup y) = -\log_2 p_Y(y)$. □

The atoms are ordered on a lattice by the partial ordering relation between atoms with antichain α and β being given by (Williams and Beer, 2010)

$$\alpha \preceq \beta \Leftrightarrow \forall \boldsymbol{b} \in \beta \; \exists \boldsymbol{a} \in \alpha \text{ such that } \boldsymbol{a} \subseteq \boldsymbol{b} \,. \tag{13}$$

The atoms are, then, computed as the Moebius inversion of the corresponding redundancies on the lattice, which is referred to throughout the literature as the Redundancy Lattice.

Lemma A.4. *The degree of synergy $m \in \mathbb{N}$ increases monotonically on the redundancy lattice, i.e., $\alpha \preceq \beta \Rightarrow m(\alpha) \leq m(\beta)$.*

Proof. Let $\alpha, \beta \in \mathcal{P}(\mathcal{P}(\{1, \ldots, n\}))$ be two antichains on the n redundancy lattice such that $\alpha \preceq \beta$. By definition of the degree of synergy (Equation (4)), there exists a set $\boldsymbol{b} \in \beta$ such that $m(\beta) = |\boldsymbol{b}|$. For this $\boldsymbol{b}$, it follows from the definition of the partial order of the antichains that there must then also exist a set $\boldsymbol{a} \in \alpha$ for which $\boldsymbol{a} \subseteq \boldsymbol{b}$. Thus, $\alpha \preceq \beta \Rightarrow m(\alpha) \leq |\boldsymbol{a}| \leq |\boldsymbol{b}| = m(\beta)$. □

Theorem A.4. *The representational complexity of a categorical random variable Y and its one-hot representation is equal to one.*

Proof. The local mutual information of the event $(T = t, S = s)$ amounts to $i(y : \vec{y}) = -\log_2(p_Y(y))$ and is thus equal to the local redundancy $i^{\text{sx}}_{\cap}(y_j : \vec{y}_{\alpha_j})$ (Lemma A.3). Because all local atoms are non-negative (Proposition A.1), all local atoms π with antichains β succeeding α_j must be zero. Since $m(\alpha_j) = 1$ and $m(\beta) = 1$ for all $\beta \preceq \alpha$ (Lemma A.4), the representational complexity of the one-hot encoding is $C = 1$. □

A.5 DNN implementation

A.5.1 MNIST feedforward deep neural network

The MNIST networks analyzed in this paper are fully-connected feed-forward deep neural networks with quantized activation values, but float-precision weights. These networks are trained on the 60000 28x28 grayscale pictures of handwritten digits of the training set of the MNIST dataset (LeCun et al., 1998). To get better statistics for the test error, the 60000 test samples of the QMNIST dataset have been utilized (Yadav and Bottou, 2019). The networks use tanh activation functions on the hidden layers, while on the output layer employing a softmax (for one-hot output layer) or sigmoid (for binary output layer).

A total of three different networks have been trained with 20 different random weight initializations each: Figures 3.B and 4.A have been computed on networks trained and evaluated with eight quantization levels per neuron but with different output layer representations: While the networks represented in Figure 3.B have a ten-neuron one-hot output layer, the networks whose results are depicted in Figure 4.A have only four output neurons of which each represents one bit of the binary representation of the numeric label. While the networks shown in Figures 5.B and D share the same network architecture as the ones in Figure 3, they have been trained and evaluated with only four quantization levels to make the computation of the coarse-grained PID more efficient.

For all networks, we used stochastic gradient descent with a batch size of 64, learning rate of 0.01 and Xavier weight initialization. The networks with one-hot output representation employ a cross-entropy loss, while for the binary representation, a mean square error loss was chosen. Parameters and accuracies of the networks are summarized in Table 1.

Network	#runs	#quantization levels	Output rep. (#neurons)	train acc.	test acc.
Default	20	8	one-hot (10)	99.96(2)	95.0(4)
Binary	20	8	binary (4)	99.59(4)	95.4(2)
Reduced	20	4	one-hot (10)	99.80(8)	94.7(4)

Table 1: Network parameters and final accuracies for the three MNIST fully-connected DNNs referenced in this paper.

A.5.2 CIFAR10 convolutional neural network

For the more complex CIFAR10 image classification task (Krizhevsky, 2009) we employed a larger feed-forward neural network with convolutional layers. The 50000 32x32x3 pictures are fed into three convolutional layers with 32, 64 and 128 filters, respectively and a kernel size of 3. The layers employ max pooling and ReLU activation functions. Afterwards, the result is flattened to 2048 numbers and fed into the fully-connected part of the network consisting of four layers with a width of 128, 32, 5, and 5, respectively, with tanh activation functions. These fully-connected layers are quantized using 8 quantization levels. Finally, the results are fed into the 10 neuron one-hot output layer.

Similar to the MNIST networks, the CIFAR10 network has been trained using stochastic gradient descent with a batch size of 64, a learning rate of 0.005, Xavier weight initialization and cross-entropy loss.

To analyze artificial neural networks using information-theoretic tools, we developed the nninfo python package. The package will be published on GitHub after the review process has concluded to preserve the authors' anonymity.

A.5.3 Quantization schemes

In order to limit the information capacity of the networks, the activation values have been quantized to very few discrete values. For evaluation, the quantized activations ℓ are computed from the continuous values $\hat{\ell}$ as

$$\ell = \epsilon \left\lfloor \frac{\hat{\ell} - \sigma_{\min}}{\epsilon} \right\rceil + \sigma_{\min} \,, \tag{14}$$

where $\lfloor\cdot\rceil$ denotes rounding to the closest integer, the bin size ϵ is given by $\epsilon = (\sigma_{\max} - \sigma_{\min})/(n_{\text{bins}} - 1)$ and $\sigma_{\min}$ and $\sigma_{\max}$ are the bounds of the activation function. This quantization scheme has been chosen as it reproduces the bounds exactly, i.e., $\hat{\ell} = \sigma_{\min/\max} \to \ell = \sigma_{\min/\max}$, and limits the rounding error to $\epsilon/2$.

For the training phase, the activation values of the forward pass are stochastically to make the training more robust. The stochastic scheme builds on the deterministic scheme presented before in that it rounds the values to the same value. However, whether values are rounded up or down to the nearest rounding point is no longer deterministic but given by a probability scaling linearly with the distance from the next two rounding points, giving

$$\ell = \epsilon\lambda + \sigma_{\min} \quad \text{where} \quad \lambda = \begin{cases} \left\lceil \frac{\hat{\ell}-\sigma_{\min}}{\epsilon} \right\rceil & r > \left(\frac{\hat{\ell}-\sigma_{\min}}{\epsilon} \mod 1 \right) \\ \left\lfloor \frac{\hat{\ell}-\sigma_{\min}}{\epsilon} \right\rfloor & r \leq \left(\frac{\hat{\ell}-\sigma_{\min}}{\epsilon} \mod 1 \right) , \end{cases} \tag{15}$$

and $r \in [0, 1]$ is drawn i.i.d. from a uniform distribution for each neuron and each evaluation.